Journal of Materials Chemistry A

ROYAL SOCIETY OF CHEMISTRY

PAPER

View Article Online
View Journal | View Issue

Check for updates

Cite this: *J. Mater. Chem. A*, 2025, **13**, 33356

Ternary strategy for energy loss suppression toward efficient rigid and flexible organic solar cells

Ruxue Ding,[a] Siying Wang,[a] Zhenyuan Yang,[b] Jiali Weng,[c] Congqi Li,[a] Zhengqi Liu,[a] Ziyang Zhang,[a] Jianqi Zhang,[d] Zheng Tang,[c] Yunhao Cai *[a] and Hui Huang *[ae]

Minimizing energy loss is critical for enhancing the efficiency of organic solar cells (OSCs), particularly for flexible applications where the voltage loss tends to be more severe. In this work, we demonstrate a high-efficiency ternary OSC by incorporating a non-fullerene small molecule, ZY-4Cl, into the PM6:L8-BO blend. The introduction of ZY-4Cl extends the absorption window and establishes a favorable energy cascade with PM6 and L8-BO. Furthermore, ZY-4Cl mitigates trap states and improves film morphology, which collectively suppress charge recombination and enhance the open-circuit voltage (V_{oc}) of OSCs. The ternary system also exhibits reduced energetic disorder and lower non-radiative recombination loss, as confirmed by a series of spectroscopic and transient characterizations. As a result, the optimized ternary device achieves an efficiency of 19.90% with a significantly elevated V_{oc}. Notably, the ternary strategy is successfully applied to flexible substrates, yielding a high efficiency of 18.51%, which is among the highest values reported for flexible OSCs, while maintaining superior voltage output. This study highlights the synergistic benefits of ternary blend engineering for simultaneously improving V_{oc}, short-circuit current, and fill factor, offering new insights into energy loss reduction and advancing the practical deployment of high-performance rigid and flexible OSCs.

Received 25th May 2025
Accepted 4th August 2025

DOI: 10.1039/d5ta04207k

rsc.li/materials-a

Yunhao Cai

Yunhao Cai is an Assistant Professor at the School of Materials Science and Opto-Electronic Technology, University of the Chinese Academy of Sciences. She received her PhD in Chemistry and Environmental Science from Beihang University in 2019, and subsequently conducted post-doctoral research in the same group. Her current research focuses on organic photovoltaic materials and devices.

Introduction

Organic solar cells (OSCs) have garnered significant attention as a next-generation photovoltaic technology for their unique advantages, including mechanical flexibility, low weight, compatibility with low-temperature solution processing, and suitability for scalable manufacturing *via* roll-to-roll printing techniques.[1–3] These attributes collectively position OSCs as a compelling candidate for emerging energy applications, particularly in the realms of wearable electronics, integrated energy systems, as well as lightweight and portable power sources.[4] Given the increasing global energy demands and escalating environmental concerns, the advancement of high-efficiency, flexible OSCs is desirable and necessary.

To date, state-of-the-art OSCs have predominantly adopted bulk heterojunction (BHJ) architectures based on donor–acceptor binary blends.[5–7] Through rational molecular design strategies and precise morphological control, the power

[a]*College of Materials Science and Opto-Electronic Technology University of Chinese Academy of Sciences, Beijing 100049, P. R. China. E-mail: caiyunhao@ucas.ac.cn; huihuang@ucas.ac.cn*

[b]*Department of Materials Science and Engineering, University of Toronto, 184 College Street, Suite 140, Toronto, Ontario M5S3E4, Canada*

[c]*State Key Laboratory for Modification of Chemical Fibers and Polymer Materials, Center for Advanced Low-Dimension Materials, College of Materials Science and Engineering Donghua University, Shanghai 201620, P. R. China*

[d]*CAS Key Laboratory of Nanosystem and Hierarchical Fabrication, CAS Center for Excellence in Nanoscience, National Center for Nanoscience and Technology, Beijing 100190, China*

[e]*School of Chemical Engineering and Technology, State Key Laboratory of Chemical Engineering and Low-Carbon Technology, Tianjin University, Tianjin 300072, China*

conversion efficiencies (PCEs) of OSCs have witnessed remarkable improvements.[8–15] Nevertheless, a major impediment to further progress lies in the persistent energy loss (E_{loss}), with open-circuit voltages (V_{oc}) typically limited to ~0.9 V, which is significantly lower than those of inorganic counterparts, such as silicon or perovskite solar cells.[16–24] This voltage deficiency originates primarily from non-radiative recombination losses, which are intrinsically linked to suboptimal molecular packing, trap-assisted recombination arising from morphological imperfections, and energetic disorder.[25–29] These challenges are further exacerbated in flexible configurations, where mechanical deformation and the intrinsic properties of flexible substrates often intensify charge recombination pathways, leading to additional V_{oc} degradation and compromised device performance.[30–33]

Ternary strategy has emerged as a promising approach to address the critical challenge of energy loss in OSCs.[34,35] By incorporating an appropriate third component into the binary active layer, this strategy not only broadens the absorption spectrum and optimizes blend morphology,[36–39] but also allows for precise tuning of the energy levels, thereby reducing both radiative and non-radiative voltage losses.[40–45] In this study, we introduce a non-fullerene acceptor, ZY-4Cl, into the well-established PM6:L8-BO system to construct a ternary blend that reduces energy loss while enhancing photovoltaic performance. ZY-4Cl exhibits complementary absorption characteristics and a higher lowest unoccupied molecular orbital (LUMO) level than L8-BO, facilitating the formation of a favorable energy cascade that enhances charge separation and boosts the V_{oc}. Furthermore, the introduction of ZY-4Cl mitigates trap-assisted recombination by reducing defect states and improves the blend morphology, collectively minimizing non-radiative recombination losses. As a result, the optimized ternary device achieves an impressive PCE of 19.90%, accompanied by simultaneous improvements in short-circuit current (J_{sc}), V_{oc}, and fill factor (FF) compared to its binary counterpart. Notably, this ternary strategy also demonstrates excellent performance in flexible devices, achieving a high PCE of 18.51%. This study underscores the potential of ternary blend engineering as an effective strategy to mitigate energy loss and enhance the efficiency of both rigid and flexible OSCs.

Results and discussion

The chemical structures of PM6,[60] L8-BO[61] and ZY-4Cl[53] are shown in Fig. 1a. The UV-visible absorption spectra of the neat films and the blend films are shown in Fig. 1b and c. It can be seen from Fig. 1b that the absorption of PM6 and L8-BO mainly locate at 500–700 nm and 600–900 nm, respectively. The absorption of ZY-4Cl complements well with those of PM6 and L8-BO, which could afford a higher J_{sc} in the corresponding ternary device. Besides, compared to the binary blends, the ternary blend exhibited a higher absorption coefficient (Fig. 1c), which indicates improved light-harvesting capability. Compared to L8-BO, ZY-4Cl showed an up-shifted LUMO energy level of −3.67 eV. The addition of ZY-4Cl made the LUMO energy cascade in the ternary system, which is beneficial to improve the V_{oc} of the ternary device (Fig. 1d).[46,47]

To investigate the influence of the third component on the photovoltaic performance of OSCs, the binary and ternary devices with the structure of indium tin oxide (ITO)/2PACz (10 nm)/active layer (100 nm)/PNDIT-F3N (10 nm)/Ag were fabricated. The weight ratio of donor and acceptor in the devices was maintained at 1 : 1.2. Diiodomethane (DIM) was used as the

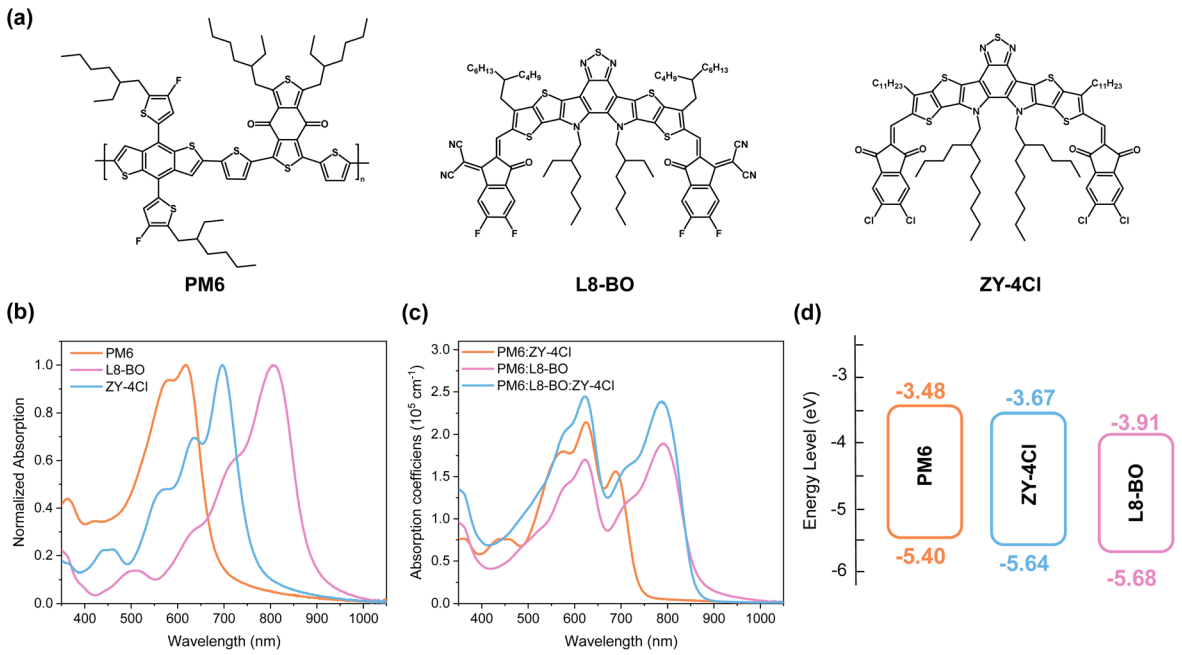

Fig. 1 (a) Chemical structures of PM6, L8-BO and ZY-4Cl. (b) Absorption spectra of PM6, L8-BO and ZY-4Cl films. (c) Absorption coefficients of binary and ternary blend films. (d) Energy level diagram for PM6, L8-BO and ZY-4Cl.

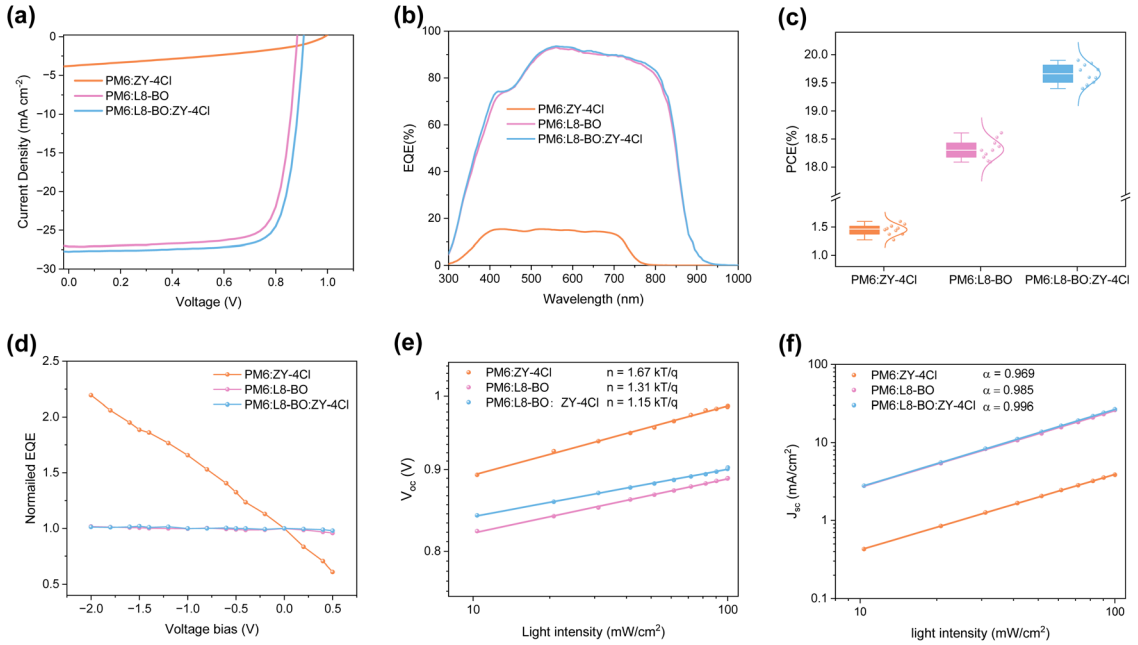

Fig. 2 (a) *J–V* characteristics and (b) EQE spectra of the binary and ternary devices. (c) The boxplot of PM6:ZY-4Cl, PM6:L8-BO, and PM6:L8-BO:ZY-4Cl devices. (d) Voltage-bias dependent EQE, (e) V_{oc} *versus* light intensity and (f) J_{sc} *versus* light intensity characteristics of the binary and ternary devices.

additive, while PM6, L8-BO, and ZY-4Cl were dissolved in chloroform. The detailed device fabrication process is shown in the SI. The current density–voltage (*J–V*) characteristics of the binary and ternary devices are shown in Fig. 2a and S1. The corresponding device parameters are shown in Table 1. The PCEs of PM6:L8-BO and PM6:ZY-4Cl devices were 18.61% and 1.6%, with V_{oc} of 0.883 V and 1.04 V, respectively. It is evident that the high V_{oc} of the PM6:ZY-4Cl device is the main contributing factor to the higher V_{oc} achieved in the ternary device when compared to the binary PM6:L8-BO device. The ternary blends with different contents of ZY-4Cl were prepared, and the *J–V* curves and device parameters are summarized in Fig. S1 and Table S1. V_{oc} was found to increase progressively as the ZY-4Cl content continuously increased. When the content of ZY-4Cl is 6 wt%, the ternary device achieved a champion PCE of 19.90%, with a J_{sc} of 27.51 mA cm^{-2}, a V_{oc} of 0.908 V and an FF of 79.67%. The binary blending ratio is 1 : 1.2 (PM6:L8-BO), and the optimum ternary blending ratio is 1 : 1.13 : 0.07 (PM6 : L8-BO : ZY-4Cl). The external quantum efficiency (EQE) spectra of the binary and ternary devices are depicted in Fig. 2b. Compared to the PM6:L8-BO binary device, the ternary device shows a slightly higher integrated J_{sc} of 27.51 mA cm^{-2}, which is well consistent with the *J–V* curve result. Fig. 2c is the boxplot of PCE, showing that the ternary device has a higher PCE and more uniform PCE distribution.

To assess the exciton dissociation and charge extraction properties, voltage-bias and light-bias EQE (response at 620 nm) were performed.[48,49] The flatter EQE value indicates that the exciton dissociation efficiency is closer to 1. As shown in Fig. 2d and S3. The PM6:L8-BO and PM6:L8-BO:ZY-4Cl devices exhibit negligible bias dependence, indicating efficient exciton dissociation and minimal bimolecular recombination, even under short-circuit conditions. In contrast, the PM6:ZY-4Cl device shows a strong dependence on both voltage and light intensity, implying inefficient exciton separation and enhanced recombination losses.

To explain and analyze the improvement of device performance, we measured the dependence of V_{oc} and J_{sc} on the light intensity (P_{light}) by analyzing the effect of the third component ZY-4Cl on the charge recombination kinetics in the device. As shown in Fig. 2e, there is a logarithmic relationship between V_{oc} and P_{light} in the device. A slope equal to 1.0 kT/q suggests a bimolecular recombination mechanism (where k is the Boltzmann constant, T is the Kelvin temperature and q is the

Table 1 Photovoltaic device parameters of binary and ternary devices

Active layer	V_{oc} (V)	J_{sc} (mA cm^{-2})	FF (%)	PCE[a] (%)
PM6:ZY-4Cl	1.040 (1.020 ± 0.003)	3.68 (3.55 ± 0.25)	41.69 (41.28 ± 0.91)	1.60 (1.44 ± 0.23)
PM6:L8-BO	0.883 (0.882 ± 0.002)	27.11 (26.98 ± 0.22)	77.73 (77.52 ± 0.30)	18.61 (18.45 ± 0.19)
PM6:L8-BO:ZY-4Cl	0.908 (0.907 ± 0.002)	27.51 (27.43 ± 0.16)	79.67 (79.51 ± 0.22)	19.90 (19.76 ± 0.18)

[a] Average values with standard deviation were obtained from 15 devices.

elementary charge).[59] For trap-assisted recombination, a higher dependence of the V_{oc} on the light intensity (>kT/q) will be observed.[40,50] It is found that the fitting slope of the ternary system is 1.15 kT/q, which is lower than that of PM6:L8-BO (1.31 kT/q) and PM6:ZY-4Cl (1.67 kT/q). This indicates that the introduction of the third component reduces the trap-assisted recombination in the device as well as the non-radiative recombination of charge carriers during the transport process.[51] In the ternary device, $J_{sc} \propto P_{light}^{\alpha}$ is closer to 1, suggesting less bimolecular recombination. As shown in Fig. 2f, the slope values of the devices based on the PM6:L8-BO and PM6:L8-BO:ZY-4Cl are 0.985 and 0.996, respectively. Therefore, it can be inferred that compared with the PM6:L8-BO, the introduction of ZY-4Cl suppresses the bimolecular recombination and further helps to improve the J_{sc} and FF of the device.

The space charge limited current (SCLC) method was used to explore the charge carrier mobilities in the device (Fig. S4). The hole-transport and electron-transport devices were fabricated following the procedures detailed in SI. The hole mobility (μ_h) and electron mobility (μ_e) values are shown in Table S2. The incorporation of ZY-4Cl increases the μ_h and μ_e values of the ternary system. Compared with the PM6:L8-BO binary system, the μ_h value increases from 3.43×10^{-4} cm^2 V^{-1} s^{-1} to 4.22×10^{-4} cm^2 V^{-1} s^{-1}, and the μ_e increases from 3.28×10^{-4} cm^2 V^{-1} s^{-1} to 4.13×10^{-4} cm^2 V^{-1} s^{-1}. The higher hole and electron mobilities indicate that the addition of ZY-4Cl can facilitate the J_{sc} of the device. Compared with the PM6:L8-BO device ($\mu_h/\mu_e = 1.05$) and the PM6:ZY-4Cl device ($\mu_h/\mu_e = 1.30$), the μ_h/μ_e of the PM6:L8-BO:ZY-4Cl device is 1.02, suggesting that the ternary blend has a more balanced charge transport, consistent with the highest performance achieved in the ternary device. In addition, we calculate the trap state (n_t), which is related to carrier recombination and carrier transport. The trap state is calculated by $V_{TFL} = \frac{en_tL^2}{2\varepsilon\varepsilon_0}$, where e is the charge, L is the thickness of the active layer, and ε and ε_0 are the relative dielectric constant and vacuum dielectric constant. According to the hole-only device diagram, we found that the curve is divided into three sections. The first section ($n = 1$) is the linear region, where the current is limited by the carrier injection. The second section ($n > 3$) forms a fast-growing nonlinear region with the increase of voltage. The carrier in this region is affected by the recombination mechanism, and the turning point of the two sections is V_{TFL}. It is found that the n_t of the PM6:L8-BO:ZY-4Cl is 1.53×10^{16} cm^{-3}, which is lower than the PM6:L8-BO (1.60×10^{16} cm^{-3}). The smaller defect state density is beneficial to reduce the charge recombination and improve the device efficiency.

ZY-4Cl and L8-BO may have good compatibility due to the partial similarity of their chemical structures. Therefore, the contact angle test was carried out, and the results are shown in Fig. S5 and Table S3. The contact angles of the PM6, L8-BO and ZY-4Cl neat films were tested on water and ethylene glycol, respectively. Using the Wu's model, the γ values of PM6, L8-BO and ZY-4Cl were calculated to be 21.9 mN m^{-1}, 30.2 mN m^{-1}, and 28.6 mN m^{-1}, respectively. The compatibility between the materials is calculated from the equation of $\chi \propto (\sqrt{\gamma_A} - \sqrt{\gamma_B})^2$, where χ is the Flory–Huggins interaction parameter representing the degree of intermolecular interaction.[25] The χ of L8-BO/ZY-4Cl is as small as 0.02 mN m^{-1}. The results showed that L8-BO and ZY-4Cl have good affinity, allowing for easy homogeneous phase formation in the ternary system.[54]

The film morphology significantly impacts the photovoltaic performance of the device, influencing charge generation, transport, and collection efficiencies. The thin-film morphology was characterized using atomic force microscopy (AFM) and grazing-incidence wide-angle X-ray scattering (GIWAXS) to investigate its microstructure and molecular packing orientation. Fig. 3a and S6 show the height and phase images of the PM6:ZY-4Cl, PM6:L8-BO, and PM6:L8-BO:ZY-4Cl films. It can be seen that the PM6:ZY-4Cl film shows the lowest root mean square (RMS) roughness value among these blend films. Compared with the PM6:L8-BO film, the PM6:L8-BO:ZY-4Cl film shows a larger RMS value. Moreover, the ternary blend film exhibits more obvious fibrillar morphology compared to the binary counterparts. This optimized microstructure facilitates improved charge separation and transport within the active layer, ultimately leading to enhanced J_{sc} and FF.[52] We also performed AFM-IR to provide insights into donor–acceptor distribution and phase separation behavior in the ternary blend. As shown in Fig. S7g–i, PM6, L8-BO, and ZY-4Cl form a fibrous network structure in the blend film. Compared to the binary blend film, the PM6:L8-BO:ZY-4Cl ternary blend film exhibits more distinct nanofibrillar structures, forming an interpenetrating nano-network. This indicates that the addition of ZY-4Cl not only enhances the crystallinity of the film but also providing a more favorable microstructure for charge separation and transport. Furthermore, analysis of the fiber width (full width at half maximum, FWHM) in the blend film (Fig. S11). The PM6:L8-BO:ZY-4Cl film has fiber diameters of 22.9 nm (donor) and 22.4 nm (acceptor), which are larger and more closely matched than the binary blend film. This improved morphological compatibility facilitates efficient exciton dissociation and charge transport.

2D GIWAXS patterns of the neat PM6, L8-BO and ZY-4Cl are shown in Fig. S12a. The corresponding linear cutting intensities in the in-plane (IP) and out-of-plane (OOP) directions are displayed in Fig. S12b. The 2D GIWAXS patterns of both L8-BO and ZY-4Cl show distinct arc-shaped signals along the q_z direction, indicating a predominant face-on molecular orientation in these acceptor materials. The GIWAXS images and intensity distributions of PM6:ZY-4Cl, PM6:L8-BO, and PM6:L8-BO:ZY-4Cl are shown in Fig. 3b and c. The PM6:L8-BO binary film exhibits distinct molecular packing characteristics: L8-BO shows a (010) π–π stacking peak at 1.733 Å^{-1} in the out-of-plane direction, and PM6 displays a (100) diffraction peak at 0.305 Å^{-1} in the in-plane direction. Notably, the ternary blend maintains this preferential face-on orientation after ZY-4Cl incorporation, as evidenced by the preserved diffraction features. This demonstrates that ZY-4Cl introduction minimally perturbs the molecular packing arrangement of the host system. Comparative analysis of GIWAXS patterns between

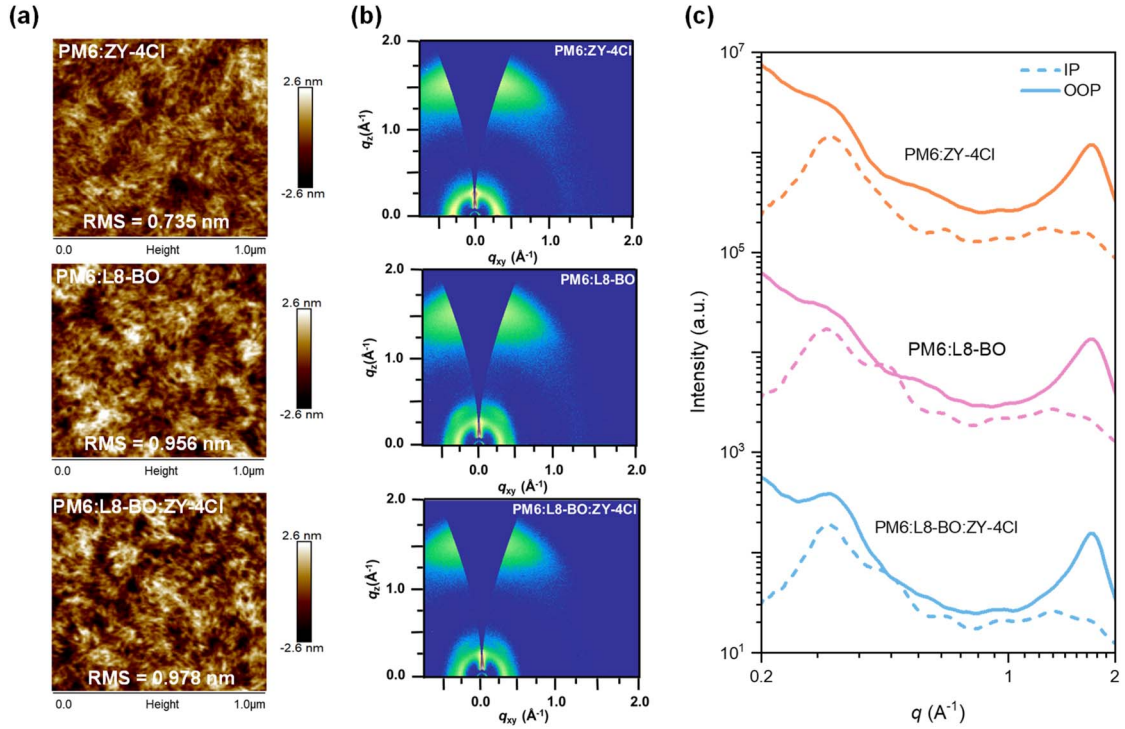

Fig. 3 (a) AFM height images (1 μm × 1 μm). (b) 2D GIWAXS patterns and (c) the corresponding in-plane and out-of-plane line-cut profiles of the binary and ternary blend films.

binary and ternary blend films revealed enhanced structural ordering in the ternary system, with increased intensities of the lamellar stacking and π–π packing peaks. The detailed crystal coherence length (CCLs) of the blends are summarized in Table S5. The CCL associated with the lamellar stacking increased from 80.51 Å to 98.13 Å and the π–π stacking increased from 25.32 Å to 28.16 Å. These enhanced CCL values demonstrate that ZY-4Cl incorporation promotes tighter molecular packing between donor and acceptor components. This improved structural ordering facilitates more efficient electron transport within the active layer.

Energy loss (E_{loss}) analysis was performed to explore the reasons for the high V_{oc} achieved in the ternary device, as shown in Fig. 4a–c. E_{loss} parameters are shown in Table 2. The E_{loss} of the device is composed of three parts. The first part (ΔE_1) is caused by the gap between the band gap (E_g) and the upper limit of the open circuit voltage (V_{sq}^{oc}), which is determined by the Shockley–Queisser limit. ΔE_1 and ΔE_2 together constitute the radiation loss of the device. The third part (ΔE_3) is non-radiative energy loss, which is also the main factor of energy loss in OSC. The specific expression is as follows:

$$E_{loss} = E_g - qV_{loss} = (E_g - qV_{sq}^{oc}) + (qV_{sq}^{oc} - qV_{rad}^{oc}) + (qV_{rad}^{oc} - qV_{oc}) = \Delta E_1 + \Delta E_2 + \Delta E_3 \quad (1)$$

The PM6:L8-BO system and the PM6:L8-BO:ZY-4Cl system have similar E_g and the same V_{sq}^{oc} (1.175 eV). Therefore, ΔE_1 is not the main reason for the high V_{oc} of the ternary device. The V_{rad}^{oc} was calculated by high sensitivity EQE, since:

$$J_{rad}^0 = \int EQE_{PV} \times BBdE \quad (2)$$

$$V_{rad}^{oc} = kT/q \ln(J_{ph}/J_{rad}^0) \quad (3)$$

The EQE spectra and EL curves of the PM6:L8-BO system and the PM6:L8-BO:ZY-4Cl system are comparable, with V_{rad}^{oc} values of 1.126 eV and 1.128 eV, respectively. The ΔE_2 of the ternary system (0.047 eV) is lower than the binary system (0.050 eV).

Fig. 4d is the external quantum efficiency of electroluminescence (EQE_{EL}), which was used to analyze the reduction of non-radiative energy loss. It was found that the PM6:L8-BO:ZY-4Cl system had a higher EQE_{EL} value (1.996×10^{-4}) than the PM6:L8-BO system (1.705×10^{-4}). According to the equation of $\Delta E_3 = qV_{rad}^{oc} - qV_{oc}$, ΔE_3 of the binary and ternary devices are 0.238 and 0.220 eV. Therefore, the introduction of ZY-4Cl into the PM6:L8-BO reduces the non-radiative energy loss in the device, and the E_{loss} is reduced from 0.553 eV to 0.532 eV. Fig. 5a is the calculated results of the Urbach energy (E_u). It was found that the ternary system demonstrates a lower Urbach energy (E_u = 26.21 eV) compared to the binary system (27.29 eV). This reduction in E_u indicates decreased energetic disorder within the system. The lower energetic disorder facilitates more efficient charge extraction and reduces energy losses, which is reflected in the enhanced V_{oc} and FF of the ternary device.

Transient photovoltage (TPV) and transient photocurrent (TPC) measurements were conducted to investigate the carrier recombination, extraction, and transport dynamics in the devices. Both the photovoltage decay under open-circuit conditions and photocurrent decay under the short-circuit

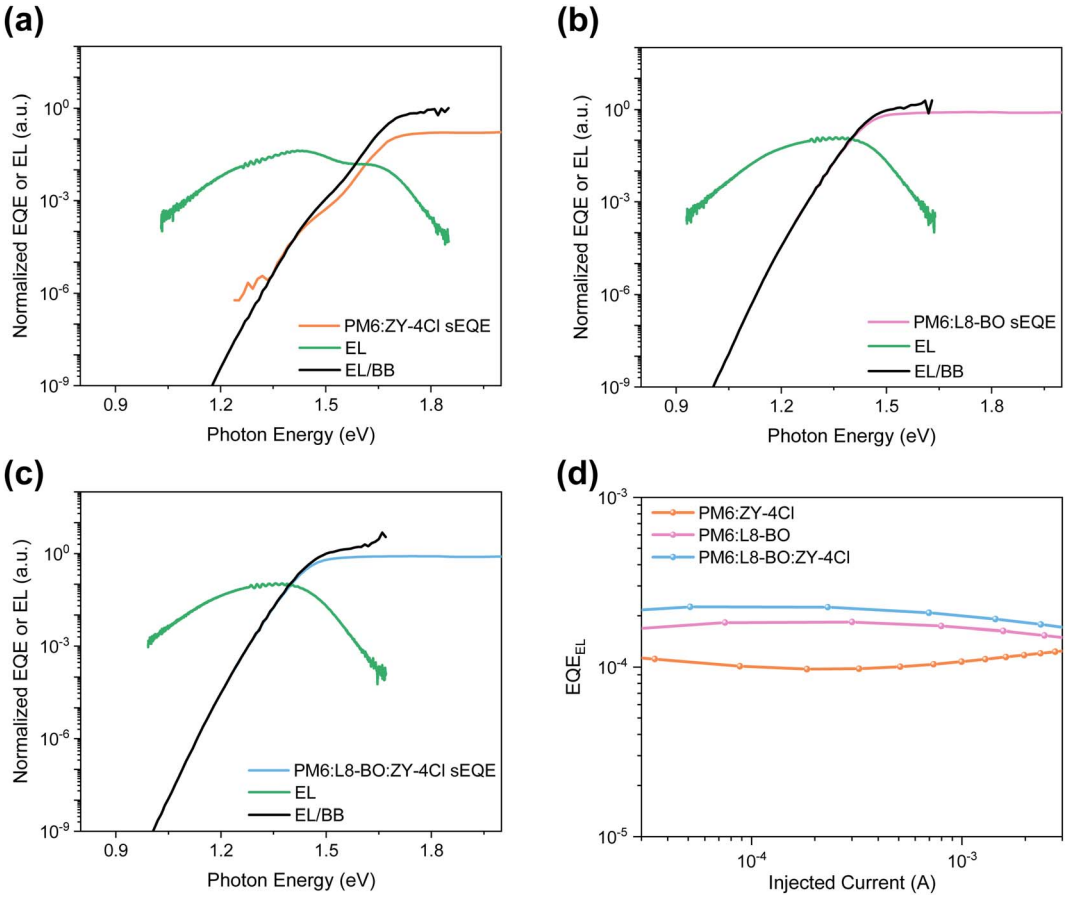

Fig. 4 Sensitive EQE and EL spectra based on the (a) PM6:ZY-4Cl, (b) PM6:L8-BO, and (c) PM6:L8-BO:ZY-4Cl devices. (d) EQE_{EL} of the binary and ternary devices.

conditions exhibit mono-exponential behavior, corresponding to the carrier recombination and extraction processes, respectively. As shown in Fig. 5c, the PM6:L8-BO:ZY-4Cl demonstrates the longest charge recombination times (12.73 μs) compared to PM6:L8-BO and PM6:ZY-4Cl (11.64 μs and 2.67 μs), indicating suppressed charge recombination and enhanced carrier survival. To further analyze the recombination dynamics, we derived the reaction order (Φ) based on the relationship between charge lifetime (τ) and V_{oc}, and between carrier density (n) and V_{oc}.[62] Specifically, we extracted β from the slope of $\log(\tau)$ *versus* V_{oc}, and γ from the slope of $\log(n)$ *versus* V_{oc} (Fig. S18c, d, S19c and d), and calculated the reaction order using the relation $\Phi = \beta/\gamma + 1$. Our results show that the reaction order of the PM6:L8-BO binary system ($\Phi = 2.53$) is slightly lower than that of the ternary system ($\Phi = 2.61$). Therefore, the actual recombination dynamics suggest that the ternary system exhibits a longer charge lifetime. This improvement can be attributed to reduced defect states and energetic disorder in the ternary blend, contributing to better photovoltaic performance. On the other hand, the charge extraction times, obtained from TPC measurements, follow a decreasing trend (0.57 μs > 0.33 μs > 0.25 μs) for PM6:ZY-4Cl, PM6:L8-BO, and PM6:L8-BO:ZY-4Cl, respectively, suggesting more efficient and faster charge extraction in the ternary device (shown in Fig. 5b). The PM6:ZY-4Cl blend shows inferior photovoltaic performance due to its higher recombination rate and slower carrier extraction. In contrast, the ternary system achieves superior charge transport capability through the synergistic combination of reduced recombination and accelerated carrier extraction.

Repeated bending stresses can induce structural modifications in flexible organic solar cells (F-OSCs), including alterations in molecular packing and intermolecular interactions

Table 2 E_{loss} related parameters of the binary and ternary devices

Active layer	E_g (eV)	V_{oc} (V)	E_{loss} (eV)	V_{rad}^{oc} (V)	V_{sq}^{oc} (V)	ΔE_1 (eV)	ΔE_2 (eV)	$\Delta E_3{}^a$ (eV)	$\Delta E_3{}^b$ (eV)	EQE_{EL}
PM6:ZY-4Cl	1.59	1.040	0.550	1.287	1.315	0.275	0.028	0.247	0.236	1.078×10^{-4}
PM6:L8-BO	1.44	0.887	0.553	1.126	1.175	0.265	0.050	0.238	0.224	1.705×10^{-4}
PM6:L8-BO:ZY-4Cl	1.44	0.908	0.532	1.128	1.175	0.265	0.047	0.220	0.220	1.996×10^{-4}

[a] Calculated using the expression $\Delta E_3 = qV_{rad}^{oc} - qV_{oc}$. [b] Calculated using the expression $\Delta E_3 = -kT\ln(EQE_{EL})$.

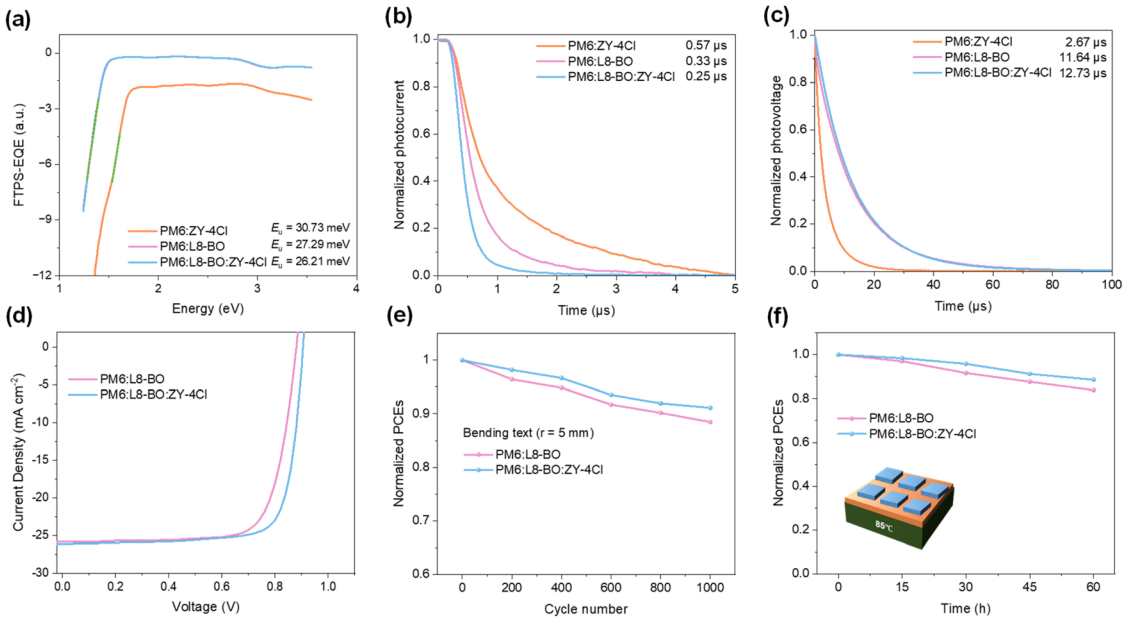

Fig. 5 (a) FTPS-EQE of the binary and ternary systems. (b) TPC and (c) TPV measurements of the binary and ternary devices. (d) *J*–*V* curves of the flexible devices based on the PM6:L8-BO and PM6:L8-BO:ZY-4Cl systems. (e) Normalized PCEs of the PM6:L8-BO and PM6:L8-BO:ZY-4Cl flexible devices after bending at 5 mm curvature radius. (f) Normalized PCEs of the unencapsulated binary and ternary devices after thermal stability tests in the dark and nitrogen atmosphere at 85 °C.

within the active layer. Such structural changes may lead to shifts in material energy levels, consequently affecting the V_{oc} of the devices.[57,58] Moreover, under harsh environmental conditions, characterized by elevated temperature and humidity, the organic components in F-OSCs demonstrate increased vulnerability to degradation. This environmental instability promotes the formation of defect states that act as charge recombination centers, ultimately compromising device performance.[55,56] Addressing these stability issues through material engineering and device optimization remains crucial for realizing the full potential and commercial viability of F-OSCs in their large-scale applications.

To address these challenges, we implemented the ternary system on flexible substrates. For the substrate selection, we employed a silver alloy-coated polyethylene terephthalate flexible electrode, which offers distinct advantages over conventional ITO substrates. Comprehensive characterization demonstrates that incorporating ZY-4Cl into the ternary system effectively optimizes the active layer morphology while simultaneously suppressing defect states and minimizing carrier recombination. These synergistic effects collectively reduce non-radiative energy losses and enhance overall photovoltaic performance. Consequently, the ternary-based F-OSC shows a high efficiency of 18.51%, with a J_{sc} of 26.11 mA cm^{-2}, a V_{oc} of 0.905 V and an FF of 78.31% (shown in Table 3). Such a PCE is among the highest value reported for F-OSCs, and markedly higher than the binary devices. Fig. 5d presents the *J*–*V* characteristics of flexible devices based on the PM6:L8-BO and PM6:L8-BO:ZY-4Cl. The improved efficiency of the ternary flexible device arises from synergistic effects including reduced voltage losses, optimized film morphology, and enhanced charge transport.

Thermal stability tests were conducted on unencapsulated devices under 85 °C in nitrogen atmosphere with complete light exclusion, as illustrated in Fig. 5f. Remarkably, the ternary system retained 88.5% of its initial PCE after 60 hours of thermal aging, outperforming the PM6:L8-BO system (83.9% retention). This demonstrates that ZY-4Cl's incorporation substantially enhances the device's thermal stability. Mechanical stability was further evaluated through bending tests with a 5 mm radius (Fig. 5e). After 1000 bending cycles, the PM6:L8-BO:ZY-4Cl device maintained 91.1% of its initial PCE, exhibiting superior mechanical robustness compared to the binary counterpart. We also conducted continuous illumination tests under standard solar intensity (1 sun) at an ambient temperature of approximately 25 °C. As shown in Fig. S22, the ternary

Table 3 Photovoltaic device parameters of the binary and ternary flexible devices

Active layer	V_{oc} (V)	J_{sc} (mA cm^{-2})	FF (%)	PCE[a] (%)
PM6:L8-BO	0.880 (0.878 ± 0.004)	25.78 (25.58 ± 0.36)	75.26 (75.05 ± 0.43)	17.08 (16.89 ± 0.22)
PM6:L8-BO:ZY-4Cl	0.905 (0.904 ± 0.003)	26.11 (26.01 ± 0.20)	78.31 (78.12 ± 0.37)	18.51 (18.38 ± 0.16)

[a] Average values with standard deviation were obtained from 15 devices.

device retained 80% of its initial efficiency after 372 h of continuous operation, whereas the binary device exhibited more pronounced efficiency degradation under the same conditions, with a T_{80} lifetime of 299 h. These results indicate that the ternary system exhibits improved operational stability compared to the binary system.

Conclusion

In conclusion, this work highlights a ternary strategy that effectively addresses energy loss in OSCs by incorporating the non-fullerene small molecule ZY-4Cl into the PM6:L8-BO binary system. The introduction of ZY-4Cl not only broadens the absorption spectrum but also forms a well-aligned energy cascade with PM6 and L8-BO, which facilitates more efficient charge transfer and reduces voltage loss—one of the primary factors limiting OSC efficiency. Moreover, ZY-4Cl reduces trap density and improves film morphology, leading to suppressed non-radiative recombination and prolonged carrier lifetimes. These synergistic effects contribute to a high PCE of 19.90% with a notable improvement in V_{oc}. Importantly, the ternary strategy also proven effective in flexible devices, achieving a PCE of 18.51% with an excellent voltage output, which ranks among the highest for F-OSCs. These results underscore the critical role of energy loss minimization in OSC performance optimization and demonstrate the potential of rational ternary design for advancing high-efficiency flexible photovoltaics.

Conflicts of interest

The authors declare no conflict of interest.

Data availability

All data supporting the findings of this study are available within the article. Data will available on request from the authors.

Supplementary information is available. See DOI: **https://doi.org/10.1039/d5ta04207k**.

Acknowledgements

The authors acknowledge the National Natural Science Foundation of China (52120105006, 52473200), the Fundamental Research Funds for the Central Universities (E4ER1801, E3ET1803), the Youth Innovation Promotion Association of Chinese Academy of Sciences (2022165). The authors gratefully acknowledge the assistance of Runjie Zhang and Prof. Fengjiao Zhang for the GIWAXS measurement.

References

1 M. Li, S. Feng, S. Shen, H. Huang, W. Xue, N. Yu, Y. Zhou, W. Ma, J. Song, Z. Tang and Z. Bo, *Chem. Eng. J.*, 2022, **438**, 135384.
2 G. Sun, X. Jiang, X. Li, L. Meng, J. Zhang, S. Qin, X. Kong, J. Li, J. Xin, W. Ma and Y. Li, *Nat. Commun.*, 2022, **13**, 5267.
3 S. Li, L. Zhan, Y. Li, C. He, L. Zuo, M. Shi and H. Chen, *Small Methods*, 2022, **6**, 2200828.
4 Z. Chen, J. Ge, W. Song, X. Tong, H. Liu, X. Yu, J. Li, J. Shi, L. Xie, C. Han, Q. Liu and Z. Ge, *Adv. Mater.*, 2024, **36**, 2406690.
5 X. Fan, *Adv. Funct. Mater.*, 2021, **31**, 2009399.
6 W. Zhang, W. Song, J. Huang, L. Huang, T. Yan, J. Ge, R. Peng and Z. Ge, *J. Mater. Chem. A*, 2019, **7**, 22021–22028.
7 Y. Zhu, D. He, C. Wang, X. Han, Z. Liu, K. Wang, J. Zhang, X. Shen, J. Li, Y. Lin, C. Wang, Y. He and F. Zhao, *Angew. Chem., Int. Ed.*, 2024, **63**, e202316227.
8 T. Zhang, C. An, Y. Cui, J. Zhang, P. Bi, C. Yang, S. Zhang and J. Hou, *Adv. Mater.*, 2022, **34**, 2105803.
9 X. Gao, X. Wu, Z. Wu, J. Gao and Z. Liu, *Sci. China Chem.*, 2025, **68**, 3359–3375.
10 Y. Patil, R. Misra, M. L. Keshtov and G. D. Sharma, *J. Mater. Chem. A*, 2017, **5**, 3311–3319.
11 X. Zhang, Z. Lu, L. Ye, C. Zhan, J. Hou, S. Zhang, B. Jiang, Y. Zhao, J. Huang, S. Zhang, Y. Liu, Q. Shi, Y. Liu and J. Yao, *Adv. Mater.*, 2013, **25**, 5791–5797.
12 N. Yang, S. Zhang, Y. Cui, J. Wang, S. Cheng and J. Hou, *Nat. Rev. Mater.*, 2025, **10**, 404–424.
13 X. Liu, Y. Wei, X. Zhang, L. Qin, Z. Wei and H. Huang, *Sci. China Chem.*, 2021, **64**, 228.
14 Q. Bai, Q. Liang, H. Li, H. Sun, X. Guo and L. Niu, *Aggregate*, 2025, **6**, e650.
15 K. Xian, R. Ma, K. Zhou, J. Liu, M. Gao, W. Zhao, M. Li, Y. Geng and L. Ye, *Aggregate*, 2024, **5**, e466.
16 P. Cheng and Y. Yang, *Acc. Chem. Res.*, 2020, **53**, 1218–1228.
17 A. Opitz, J. Frisch, R. Schlesinger, A. Wilke and N. Koch, *J. Electron Spectrosc. Relat. Phenom.*, 2013, **190**, 12–24.
18 J. Bertrandie, J. Han, C. S. P. De Castro, E. Yengel, J. Gorenflot, T. Anthopoulos, F. Laquai, A. Sharma and D. Baran, *Adv. Mater.*, 2022, **34**, 2202575.
19 R. Wang, J. Yuan, R. Wang, G. Han, T. Huang, W. Huang, J. Xue, H. Wang, C. Zhang, C. Zhu, P. Cheng, D. Meng, Y. Yi, K. Wei, Y. Zou and Y. Yang, *Adv. Mater.*, 2019, **31**, 1904215.
20 K. Sasitharan, J. Frisch, J. Kuličcek, A. Iraqi, D. G. Lidzey, M. Bär, B. Rezek and J. A. Foster, *Sci. Rep.*, 2024, **14**, 29559.
21 X. Li, Q. Zhang, J. Yu, Y. Xu, R. Zhang, C. Wang, H. Zhang, S. Fabiano, X. Liu, J. Hou, F. Gao and M. Fahlman, *Nat. Commun.*, 2022, **13**, 2046.
22 N. K. Elumalai and A. Uddin, *Energy Environ. Sci.*, 2016, **9**, 391–410.
23 J. Wu, H. Cha, T. Du, Y. Dong, W. Xu, C. Lin and J. R. Durrant, *Adv. Mater.*, 2022, **34**, 2101833.
24 X. Gu, X. Lai, Y. Zhang, T. Wang, W. L. Tan, C. R. McNeill, Q. Liu, P. Sonar, F. He, W. Li, C. Shan and A. K. K. Kyaw, *Adv. Sci.*, 2022, **9**, 2200445.
25 C. Li, G. Yao, X. Gu, J. Lv, Y. Hou, Q. Lin, N. Yu, M. S. Abbasi, X. Zhang, J. Zhang, Z. Tang, Q. Peng, C. Zhang, Y. Cai and H. Huang, *Nat. Commun.*, 2024, **15**, 8872.
26 D. Qian, Z. Zheng, H. Yao, W. Tress, T. R. Hopper, S. Chen, S. Li, J. Liu, S. Chen, J. Zhang, X.-K. Liu, B. Gao, L. Ouyang, Y. Jin, G. Pozina, I. A. Buyanova, W. M. Chen, O. Inganäs,

V. Coropceanu, J.-L. Bredas, H. Yan, J. Hou, F. Zhang, A. A. Bakulin and F. Gao, *Nat. Mater.*, 2018, **17**, 703–709.
27 J. Fu, P. W. K. Fong, H. Liu, C.-S. Huang, X. Lu, S. Lu, M. Abdelsamie, T. Kodalle, C. M. Sutter-Fella, Y. Yang and G. Li, *Nat. Commun.*, 2023, **14**, 1760.
28 Y. Sun, J. Liu, X. Duan, J. Zhang, Z. Ge, L. Liu, J. Qiao, Y. Li, Z. Bi, H. Zhang, J. Gao, J. Yan, S. Liu, Z. Tang, X. Hao, W. Ma, F. Gao and J. Zhang, *Angew. Chem., Int. Ed.*, 2025, e202500129.
29 Q. Liu and K. Vandewal, *Adv. Mater.*, 2023, **35**, 2302452.
30 Y. Wang, J. Yu, R. Zhang, J. Yuan, S. Hultmark, C. E. Johnson, N. P. Gallop, B. Siegmund, D. Qian, H. Zhang, Y. Zou, M. Kemerink, A. A. Bakulin, C. Müller, K. Vandewal, X.-K. Chen and F. Gao, *Nat. Energy*, 2023, **8**, 978–988.
31 M. Wang, K. Zheng and X. Cai, *Opt. Mater.*, 2025, **159**, 116639.
32 Z. Wang, Y. Han, L. Yan, C. Gong, J. Kang, H. Zhang, X. Sun, L. Zhang, J. Lin, Q. Luo and C. Ma, *Adv. Funct. Mater.*, 2021, **31**, 2007276.
33 P. Bi, S. Zhang, T. Xiao, M. Cui, Z. Chen, J. Ren, C. Qin, G. Lu, X. Hao and J. Hou, *Sci. China Chem.*, 2021, **64**, 599–607.
34 Y. Cai, Y. Li, R. Wang, H. Wu, Z. Chen, J. Zhang, Z. Ma, X. Hao, Y. Zhao, C. Zhang, F. Huang and Y. Sun, *Adv. Mater.*, 2021, **33**, 2101733.
35 X. Duan, W. Song, J. Qiao, X. Li, Y. Cai, H. Wu, J. Zhang, X. Hao, Z. Tang, Z. Ge, F. Huang and Y. Sun, *Energy Environ. Sci.*, 2022, **15**, 1563–1572.
36 Y. Wei, Y. Cai, X. Gu, G. Yao, Z. Fu, Y. Zhu, J. Yang, J. Dai, J. Zhang, X. Zhang, X. Hao, G. Lu, Z. Tang, Q. Peng, C. Zhang and H. Huang, *Adv. Mater.*, 2024, **36**, 2304225.
37 M. Günther, N. Kazerouni, D. Blätte, J. D. Perea, B. C. Thompson and T. Ameri, *Nat. Rev. Mater.*, 2023, **8**, 456–471.
38 N. Gasparini, L. Lucera, M. Salvador, M. Prosa, G. D. Spyropoulos, P. Kubis, H.-J. Egelhaaf, C. J. Brabec and T. Ameri, *Energy Environ. Sci.*, 2017, **10**, 885–892.
39 Y. Jiang, S. Sun, R. Xu, F. Liu, X. Miao, G. Ran, K. Liu, Y. Yi, W. Zhang and X. Zhu, *Nat. Energy*, 2024, **9**, 975–986.
40 B.-H. Jiang, Y.-P. Wang, Y.-W. Su, J.-F. Chang, C.-C. Chueh, M.-H. Shen, T.-S. Shieh, R.-J. Jeng and C.-P. Chen, *Sol. RRL*, 2021, **5**, 2100450.
41 P. Bi, S. Zhang, J. Ren, Z. Chen, Z. Zheng, Y. Cui, J. Wang, S. Wang, T. Zhang, J. Li, Y. Xu, J. Qin, C. An, W. Ma, X. Hao and J. Hou, *Adv. Mater.*, 2022, **34**, 2108090.
42 Z. Liu, C. Zhu, J. Xu, Y. Xu, J. Zeng, J. Wang, J. Zhang, P. Zhu, D. Wang, X. Zhou, Y. Zhang, X. Wang, L. Ying, L. Yan and B. Xu, *Nano Energy*, 2025, **137**, 110801.
43 Z. Zhang, W. Feng, Y. Zhang, S. Yuan, Y. Bai, P. Wang, Z. Yao, C. Li, T. Duan, X. Wan, B. Kan and Y. Chen, *Sci. China Chem.*, 2024, **67**, 1596–1604.
44 S. Wang, S. Wang, J. Wang, N. Yu, J. Qiao, X. Xie, C. Li, M. S. Abbasi, R. Ding, X. Zhang, Y. Han, G. Lu, J. Zhang, X. Hao, Z. Tang, Y. Cai and H. Huang, *Adv. Energy Mater.*, 2025, 2405205.
45 B. Zou, A. Liang, P. Ding, J. Yao, X. Zeng, H. Li, R. Ma, C. Li, W. Wu, D. Chen, M. Qammar, H. Yu, J. Yi, L. Guo, S. H. Pun, J. E. Halpert, G. Li, Z. Kan and H. Yan, *Angew. Chem., Int. Ed.*, 2025, **64**, e202415332.
46 T. Yan, W. Song, J. Huang, R. Peng, L. Huang and Z. Ge, *Adv. Mater.*, 2019, **31**, 1902210.
47 X. Liu, L. Wang, X. Liu, S. Li, Z. Liu and P. Chen, *Phys. Chem. Chem. Phys.*, 2024, **26**, 23487–23494.
48 J. S. Müller, M. Comí, F. Eisner, M. Azzouzi, D. Herrera Ruiz, J. Yan, S. S. Attar, M. Al-Hashimi and J. Nelson, *ACS Energy Lett.*, 2023, **8**, 3387–3397.
49 D. J. Wehenkel, K. H. Hendriks, M. M. Wienk and R. A. J. Janssen, *Org. Electron.*, 2012, **13**, 3284–3290.
50 S. Ryu, N. Y. Ha, Y. H. Ahn, J.-Y. Park and S. Lee, *Sci. Rep.*, 2021, **11**, 16781.
51 Z. Xing, X. Meng, R. Sun, T. Hu, Z. Huang, J. Min, X. Hu and Y. Chen, *Adv. Funct. Mater.*, 2020, **30**, 2000417.
52 L. Zhao, H. Wang, H. Ji, S. Li, X. Miao, C. Zhu, W. Wang, D. Huang and X. Dong, *APL Mater.*, 2023, **11**, 120601.
53 S. Zhang, Y. Meng, T. Lin, Y. Su, S. Yuan, Q. Li, B. Xiao, R. Chen, T. Jia, X. Qi, Y.-P. Cai and S. Liu, *ACS Appl. Energy Mater.*, 2024, **7**, 8894–8902.
54 J. Gao, N. Yu, Z. Chen, Y. Wei, C. Li, T. Liu, X. Gu, J. Zhang, Z. Wei, Z. Tang, X. Hao, F. Zhang, X. Zhang and H. Huang, *Adv. Sci.*, 2022, **9**, 2203606.
55 W. Song, Q. Ye, S. Yang, L. Xie, Y. Meng, Z. Chen, Q. Gu, D. Yang, J. Shi and Z. Ge, *Angew. Chem.*, 2023, **135**, e202310034.
56 Z. Luo, W. Wei, R. Ma, G. Ran, L. Huang, M. H. Jee, Z. Chen, Y. Li, W. Zhang, H. Y. Woo and C. Yang, *Adv. Mater.*, 2024, **36**, 2407517.
57 C. Wei, L. Bai, X. An, M. Xu, W. Liu, W. Zhang, M. Singh, K. Shen, Y. Han, L. Sun, J. Lin, Q. Zhao, Y. Zhang, Y. Yang, M. Yu, Y. Li, N. Sun, Y. Han, L. Xie, C. Ou, B. Sun, X. Ding, C. Xu, Z. An, R. Chen, H. Ling, W. Li, J. Wang and W. Huang, *Chem*, 2022, **8**, 1427–1441.
58 Q. Xiong, H. He and M. Zhang, *Nano-Micro Lett.*, 2022, **14**, 47.
59 X. Gu, Y. Wei, G. Lu, Z. Han, D. Zheng, G. Lu, J. Zhang, Z. Wei, Y. Cai, X. Zhang and H. Huang, *Aggregate*, 2023, **4**, e338.
60 M. Zhang, X. Guo, W. Ma, H. Ade and J. Hou, *Adv. Mater.*, 2015, **27**, 4655–4660.
61 C. Li, J. Zhou, J. Song, J. Xu, H. Zhang, X. Zhang, J. Guo, L. Zhu, D. Wei, G. Han, J. Min, Y. Zhang, Z. Xie, Y. Yi, H. Yan, F. Gao, F. Liu and Y. Sun, *Nat. Energy*, 2021, **6**, 605.
62 A. Maurano, C. G. Shuttle, R. Hamilton, A. M. Ballantyne, J. Nelson, W. Zhang, M. Heeney and J. R. Durrant, *J. Phys. Chem. C*, 2011, **115**, 5947–5957.

